Optical Properties of Dibenzo[d,d′]thieno[3,2-b;4,5-b′]dithiophene Monocrystals: The Effect of Intermolecular Interactions

Laura Alessandrini,[†] Daniele Braga,[†,‡] Abdelhafid Jaafari,[§] Luciano Miozzo,[‡] Stefano Mora,[†] Leonardo Silvestri,[†] Silvia Tavazzi,* and Abderrahim Yassar[‡]

Dipartimento di Scienza dei Materiali, Università degli Studi di Milano Bicocca, Via Cozzi 53, I-20125 Milano, Italy, ITODYS, Université Paris Diderot-Paris 7, 15 rue Jean de Baïf, 75205 Paris Cedex, France, and Faculté des Sciences et Techniques de Settat, Université Hassan 1[er], Maroc

Received: June 8, 2010; Revised Manuscript Received: September 22, 2010

The polarized UV−visible absorption spectra of dibenzo[d,d′]thieno[3,2-b;4,5-b′]dithiophene single crystals are reported and interpreted to definitively attribute the observed bands and their polarizations. The results provide information on the intermolecular interactions and on the aggregation in the condensed phase, which can be of either herringbone- or H-type, depending on the electronic transition taken into considerations, with consequences on the order and polarization of the absorption bands. A relatively easy method is also discussed to obtain information on the structural/morphological properties of different types of samples, including thin films, which have been recently proposed for high-performance organic film-effect transistors for their high ionization potential and photostability.

Introduction

Oligoacene-based materials represent the most studied and promising class of molecular organic semiconductors, used as active elements in new generations of plastic and organic electronic devices.[1−3] Pentacene, the major representative of this group, shows a hole mobility of up to few tens of $cm^2\ V^{-1}\ s^{-1}$ and has become the benchmark for organic electronics.[4] Despite its potential, pentacene and other higher acenes suffer from low environmental stability. Pentacene decomposes rapidly because it has an electron-rich central ring, which is subject to a Diels−Alder reaction with oxygen.[5] To circumvent the instability of pentacene, heteroacenes in which a carbocyclic ring or rings are replaced by a heteroaromatic group have recently emerged as a new class of organic semiconductors, and their organic field effect transistors (OFETs) are reported to show both high field effect mobility and good stability.[6] The improved stability is attributed to relatively low-lying higher occupied molecular orbital (HOMO) level, although heteroacene molecules contain highly π-extended fused aromatic rings like acene.

One of the earliest reports of a high-mobility heteroacene described the synthesis and characterization of anthradithiophene.[5] This material exhibited high air stability and good device properties in the vacuum-deposited thin film form. Thus, the anthradithiophene and alkyl derivatives combine a pentacene-like intrinsic mobility with greater solubility and oxidative stability. Gao and co-workers recently reported high field effect mobility on OFETs of dibenzo[d,d′]thieno[3,2-b;4,5-b′]dithiophene ($C_{16}H_8S_3$, DBTDT) (**1**),[7] that was first synthesized sixty years ago,[8] proposing this material as valid alternative to currently used p-type organic thin-film OFETs of pentacene.[9] In contrast to pentacene, DBTDT is much more stable against oxidation, being photoinduced decomposition the main limit of pentacene.[5,10] Neckers and co-workers reported an isomer-specific synthesis of two thieno bis(benzothiophenes): thieno[2,3-f:5,4-f]bis[1]-benzothiophene and thieno[3,2-f:4,5-f]bis[1]benzothiophene along with detailed characterization of these materials. These isomers are isoelectronic with DBTDT and pentacene and composed of well-defined alternating benzene and thiophene moieties.[11] Zhu and co-workers[12] reported the synthesis and the characterization of the linearly fused pentathienoacene in which all the carbocyclic rings of pentacene are replaced with thiophene systems.

Despite the extended π-system, the spectroscopic characterization of thieno[f,f′]bis[1]benzothiophenes, DBTBT, pentathienacene and structurally related dibenzo[b,b′] thieno[2,3-f:5,4-f′] heterocycles indicates that they possess lower HOMO energy levels and larger band gaps than pentacene. The structural and electronic properties of the single DBTDT molecule have been widely discussed by Osuna et al.,[13] together with other thiophene- and selenophene-based heteroacenes studied by UV−visible-NIR spectroscopy. The conjugation properties of these systems are discussed as deduced from Raman spectroscopy. Density functional theory calculations have been performed to identify the vibrations associated with the Raman features as well as to assess information regarding the minimum-energy molecular structure and vertical one-electron excitations giving rise to the main optical absorption bands. As discussed by the authors,[13] the stabilization of the HOMO and destabilization of the lowest unoccupied molecular orbital (LUMO) lead to a broader energy gap than that of the corresponding nonfused oligothienyl counterpart. The authors discuss the significant contribution of the sulfur atoms to molecular orbitals, concluding that these heteroacenes cannot be described simply as rigidified R-oligoheteroaromatic systems. Also Okamoto et al.[14] report a UV−vis photophysical characterization and attribute the observed absorption bands of DBTDT to vibronic transitions of the single molecule. Interestingly, these semiconductors show charge carrier mobilities comparable to those of pentacene, but have a molecular gap comparable with anthracene.

Despite their interesting properties as semiconductors, reports concerning the analysis of their optical properties are scarce.

* To whom correspondence should be addressed. Tel.: +390264485035. Fax: +30264485400. E-mail: silvia.tavazzi@unimib.it.
[†] Università degli Studi di Milano Bicocca.
[‡] Université Paris Diderot-Paris 7.
[§] Université Hassan 1[er].

10.1021/jp1052826
Published on Web 12/17/2010

SCHEME 1: Synthesis of Dibenzo[d,d′]thieno[3,2-b;4,5-b′]dithiophene (1)

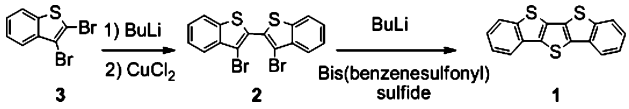

In the crystalline form, the arrangement of the DBTDT molecules has been reported by Okamoto et al.[14] No detailed studies are reported on the optical properties of the monocrystals. The UV−vis absorption of vacuum-deposited thin film is reported by Gao et al.[7] The absorption band at lowest energy of the film is found to be red shifted with respect to the band at lowest energy of the DBTDT solution. The authors tentatively attribute this effect to strong intermolecular interactions. However, the lack of a detailed analysis of the optical properties of the monocrystals did not allow the proper assignment of the optical bands.

In this paper, the polarized UV−vis absorption spectra of DBTDT single crystals are reported. The observed bands and their polarizations are definitively attributed. The results provide information on the intermolecular interactions and aggregation in the condensed phase and suggest a simple method to deduce information about the structural/morphological properties of different types of DBTDT samples, such as polycrystalline thin films, which are of special interest for device applications.

Experimental Section

The synthesis of DBTDT has been known for a long time.[15,16] An interesting route with improved yield has been recently proposed by Gao et al..[7] We followed a slightly different approach, which is shown schematically in Scheme 1. The key step of the synthesis is the ring closure reaction of the appropriate 3,3′-dibromo-2,2′-bi(benzo[b]thiophene) (**2**) with sulfur. The building block 3,3′-dibromo-2,2′-bi(benzo[b]thiophene) was prepared from 2,3-dibromobenzo[h]thiophene (**3**). The incorporation of the sulphure bridge to produce dibenzo-[d,d′]thieno[3,2-b;4,5-b′]dithiophene (**1**) was smoothly accomplished by in situ bromo-lithium exchange and reaction with bis(phenyl sulfonyl) sulphide. The yield of the reaction is 43%.

Single crystals of DBTDT were grown by the floating-drop technique of dissolving 5−6 mg of sublimated product in 3 mL of toluene.[17] The solution was filtered (size of the pores 0.2 μm), placed on the surface of water, and kept in air during solvent evaporation. Crystals grow as platelets with one accessible face for optical investigation. Single crystals were selected under crossed polarizations using an optical polarizing transmission microscope Olympus SZX12. The thickness of the crystals placed upon quartz plates was measured by atomic force microscopy (Nanoscope V Multi-Mode Veeco).

The electronic optical transitions of the isolated molecule in vacuum and the corresponding direction of polarization were calculated by means of the Gaussian 03 software, using as input parameters the molecular geometries obtained from the crystallographic data.[18] Absorbance measurements in the UV−visible spectral range were performed at room temperature using a Perkin-Elmer Lambda 900 spectrometer, equipped with Glan-Taylor calcite polarizers to vary the polarization direction of the incoming light.

Results and Discussion

DBTDT is a conjugated molecule (Figure 1) with planar conformation. The crystal structure of DBTDT is taken from

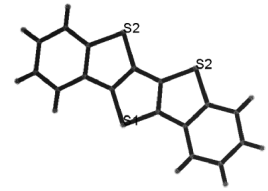

Figure 1. DBTDT molecular structure.

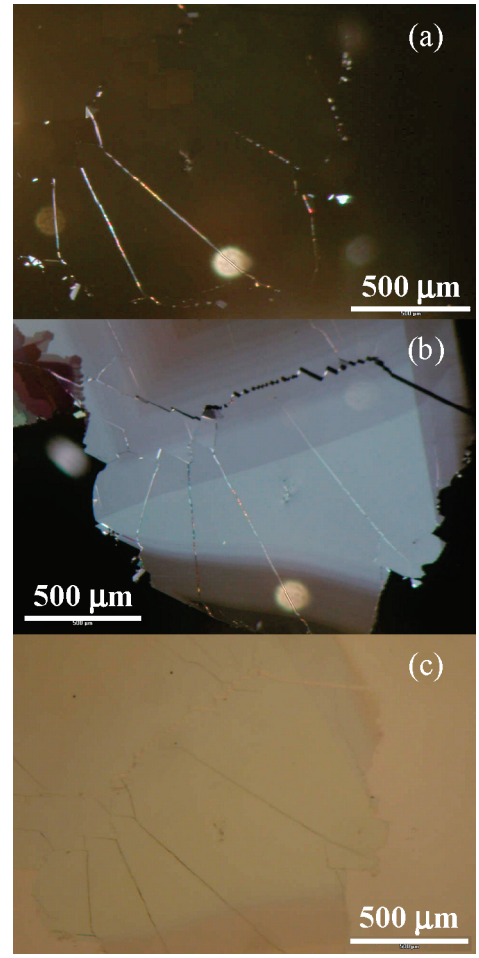

Figure 2. Images taken under the optical microscope of a DBTDT crystal with either crossed (a,b) or parallel (c) polarizer and analyzer.

the literature.[14] It is orthorhombic with cell axes $a = 7.933$ Å, $b = 26.589$ Å, and $c = 5.906$ Å and four molecules per unit cell. Figures 2, 3, and 4 show images taken under the optical microscope of DBTDT crystals. In all of the figures, the images of panels a and b were taken with crossed polarizer and analyzer, either (a) with the sample oriented to give extinction of the transmitted light or (b) for a generic orientation of the sample. The extinction is found when the electric field of the incident light is along a unit-cell axis because for orthorhombic systems the unit-cell axes are principal axes.[19] The complete extinction of the transmitted light in panels a indicates that the crystals are single. The extinction was also found by rotating the crystal of 90° around the normal to the surface (not shown here), as expected.[19] On the contrary, for a generic orientation of the sample the emerging electric field is rotated with respect to the incident electric field and the angle of rotation depends on the wavelength of light and on the crystal thickness (birefringence).[19] For this reason, the crystals are clearly distinguishable in panels b with respect to the dark background. Their uniform color and brilliance indicate that the thickness of each crystal

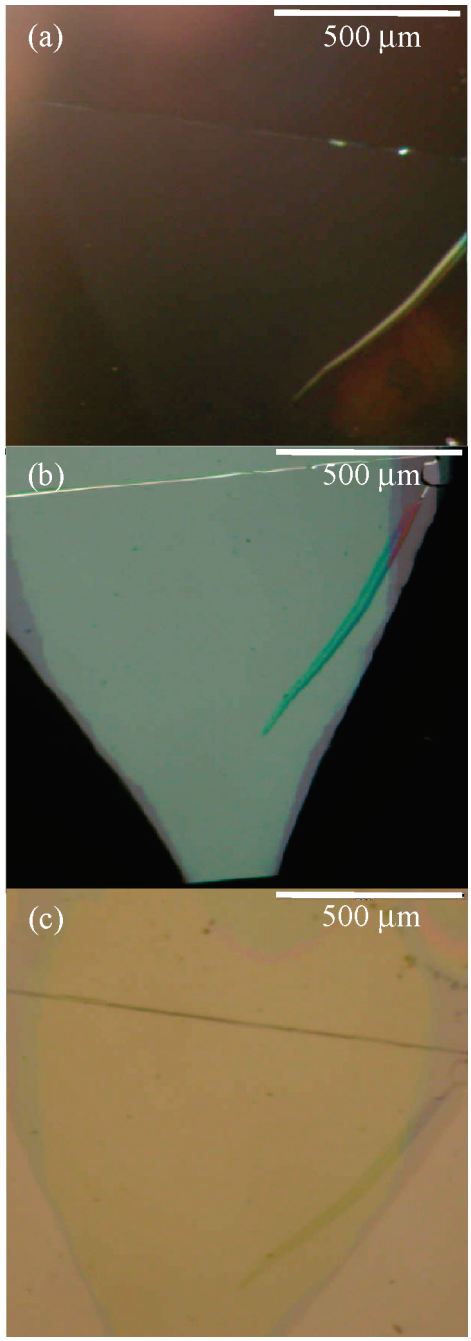

Figure 3. Images taken under the optical microscope of a DBTDT crystal with either crossed (a,b) or parallel (c) polarizer and analyzer.

is uniform in the investigated area. Finally, panels c show the images taken with parallel polarizer and analyzer. The crystals appear slightly colored (yellow due to the absorption of the complementary blue light). In particular, we selected the configuration corresponding to the incident electric field along one principal axis, the one where the absorption is larger. For the opposite case (parallel polarizer and analyzer and the incident electric field along the principal axis giving the minimum absorption, not shown here), the image of the crystal could be detected but the color is clearer and the crystal is less distinguishable with respect to the background due to its weaker absorption. Finally, the inset of Figure 4c shows the image of the corresponding sample under the atomic force microscope. Three lines on the image indicate the directions where the thickness profile was measured. A step was found, and the thickness of the sample with respect to the level of the quartz

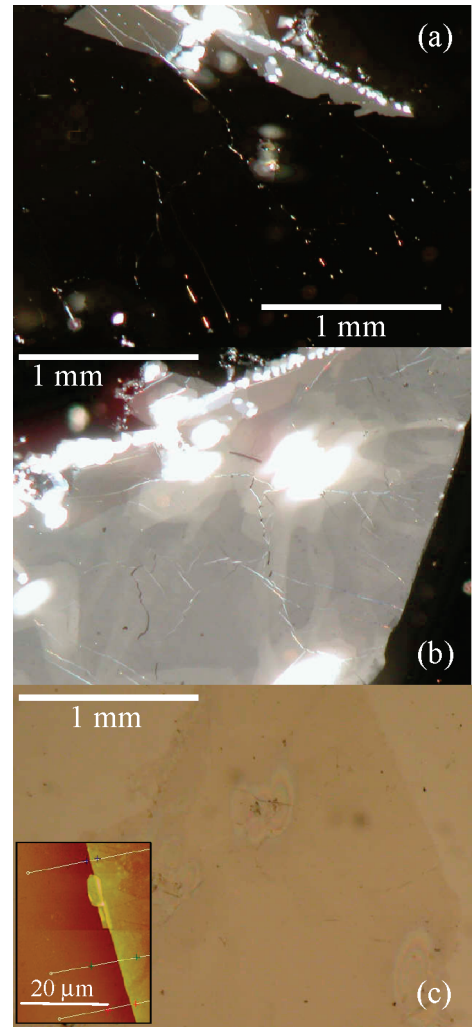

Figure 4. Images taken under the optical microscope of a DBTDT crystal with either crossed (a,b) or parallel (c) polarizer and analyzer. (Inset of c) Image under the atomic force microscope of a border of the crystal placed on a quartz substrate. The three lines indicate the three directions where the thickness profile was extracted.

substrate was found (51 ± 4) nm. This is one of the thinnest crystals that we could grow. As can be seen in Figure 4b,c, it presents few small regions where the thickness is higher (up to few hundreds of nanometers as measured by atomic force microscopy) due to the superposition of other small crystallites. These small crystallites are often misaligned with respect to the main crystal, as can be seen in Figure 4a, which shows few regions where the extinction of the transmitted light is not perfect.

Polarized absorption spectra were taken at normal incidence on the most developed face of DBTDT crystals. Figure 5 shows the spectra taken on the crystal shown in Figure 4 in the region where it is single and thin (estimated thickness equal to (51 ± 4) nm). The sample was masked thus probing an area of about 0.7−0.8 mm^2. The reported spectra were measured with two orthogonal polarizations corresponding to the extremes low- and high-energy shift of the peaks between about 3.4 and 3.8 eV (the spectra taken with intermediate polarizations are shown in the inset in a restricted energy range). These two polarizations also correspond to the two directions of the electric field that give extinction of the transmitted light under crossed polarizer and analyzer. The spectra are dominated by two orthogonally polarized vibronic series with peaks at 3.45 and 3.61 eV and a shoulder at about 3.78 eV in one case and at 3.46 and 3.62 eV

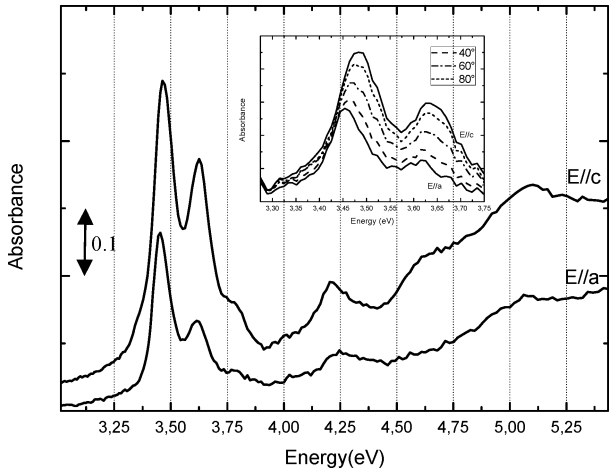

Figure 5. Absorbance spectra of the DBTDT single crystal shown in Figure 4 taken at normal incidence with two orthogonal polarizations corresponding to the extremes high-energy shift (*E*//*c*) and low-energy shift (*E*//*a*) of the peaks between about 3.4 and 3.8 eV. (Inset) Spectra taken on the same crystal with intermediate polarizations. The labels indicate the corresponding angle of the electric field to the *c* axis.

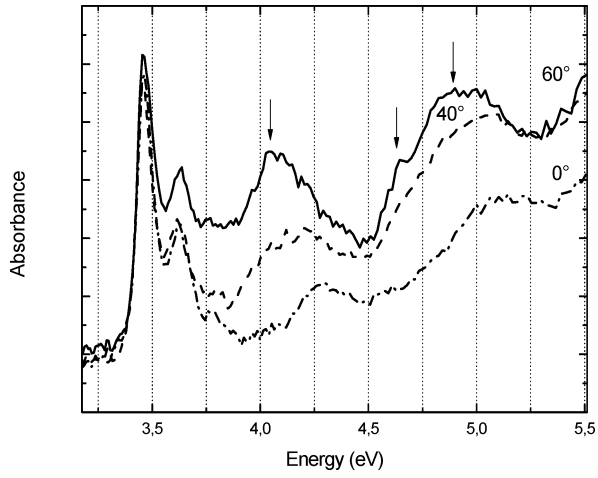

Figure 6. Absorbance spectra of the DBTDT single crystal shown in Figure 4 taken at different angles of incidence from 0 to 60° on the accessible face (*ac*) with *p* (*ab*) polarized light using the plane (*ab*) formed by the normal to the surface and the direction of polarization labeled as *E*//*a* in Figure 2 as plane of incidence.

and a shoulder at about 3.78 eV in the other case. The stronger intensity is observed in the latter case. In Figure 5, the two polarization directions are labeled *E*//*a* and *E*//*c*, since the comparison with the theoretical prediction (see below) allows deducing the corresponding polarization with respect to the axes of the crystal unit cell.

Figure 6 shows the spectra taken at oblique incidence at the angles of incidence indicated by the labels with *p*-polarized light (polarized in the plane of incidence) using, as plane of incidence, the plane formed by the normal to the surface and the direction of polarization labeled as *E*//*a* in Figure 5. Besides the replicas in the low-energy portion of the spectrum, at oblique incidence an emerging broad band is detected centered at about 4.07 eV, together with a further shoulder at about 4.6 eV and a structure at about 4.8 eV. The maximum intensity for these bands is detected for the highest angle of incidence, it decreases when decreasing the angle of incidence, and it disappears at normal incidence.

To interpret the obtained data on the single crystal, we have calculated, as a first step, the electronic optical transitions and

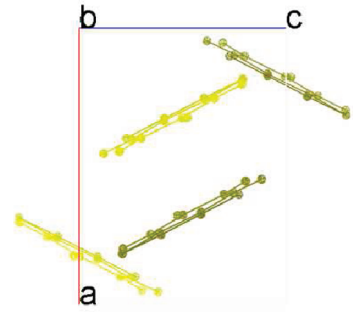

Figure 7. View of the molecular packing along the *b* crystal axis.[14]

the corresponding direction of polarization of the isolated molecule in vacuum by means of the Gaussian 03 software, using as input parameters the molecular geometries obtained from the crystallographic data.[14,18] Since our aim was the attribution of the polarized bands in the crystal, we did not optimize the molecular geometry. The obtained components of the transition moments along the inertial molecular axes (*L*, *M*, *N*, where *L* and *N* are the longest and shortest axes, respectively) are reported in Table 1, together with the available data taken from the literature for comparison.[13] The agreement with the results reported by Osuna et al.[13] is satisfactory. Spectra of DBTDT in solution have been reported by Osuna et al.[13] and the corresponding peaks of the vibronic progression have been detected at 3.62, 3.79, 3.96 eV. Also Okamoto et al.[14] report a UV−visible photophysical characterization in solution and the maximum in the absorption spectrum is reported at 344 nm (3.60 eV). The optical band observed in solution at lowest energy is attributed to the transition calculated at lowest energy, which is also the strongest one.

In principle, in the crystalline form each molecular electronic transition is predicted to give rise to four excitonic transitions.[18] We can express crystal excitonic states with a given wave vector $\mathbf{k}$ in terms of the delocalized wave functions $\Psi_{\mathbf{k},\alpha} = N^{-1/2} \Sigma_{\mathbf{n}} \exp(i\mathbf{kn})|\mathbf{n}, \alpha\rangle$, where $|\mathbf{n}, \alpha\rangle$ indicates a state in which the electronic excitation resides on molecule α in cell $\mathbf{n}$ while all other molecules in the crystal are unexcited and *N* is the total number of cells. At $\mathbf{k} = 0$, symmetry dictates that the four excitonic eigenstates are $1/2\ (\Psi_{\mathbf{k},1} + \Psi_{\mathbf{k},2} + \Psi_{\mathbf{k},3} + \Psi_{\mathbf{k},4})$, $1/2\ (\Psi_{\mathbf{k},1} - \Psi_{\mathbf{k},2} - \Psi_{\mathbf{k},3} + \Psi_{\mathbf{k},4})$, $1/2\ (\Psi_{\mathbf{k},1} - \Psi_{\mathbf{k},2} + \Psi_{\mathbf{k},3} - \Psi_{\mathbf{k},4})$, and $1/2\ (\Psi_{\mathbf{k},1} + \Psi_{\mathbf{k},2} - \Psi_{\mathbf{k},3} - \Psi_{\mathbf{k},4})$. The unit cell dipole moments of the excitonic transitions at $\mathbf{k} = 0$ are given in Table 1. In the crystal, the *L* molecular axes of all the four molecules in the unit cell are parallel to *b*, so that *L* polarized molecular transitions give rise to a pure H aggregate and only one allowed *b* polarized excitonic transition.[18] On the contrary, for all the molecular *M* polarized transitions, the arrangement in the crystal is of herringbone type. The *M* molecular axes of the four molecules in the unit cell lie in the *ac* plane and form an angle of absolute value 27° with the *c* axis. As a consequence, each *M* polarized molecular transition gives rise to two allowed excitonic transitions polarized along the *a* and *c* axes with significant projections along both the axes. The intensity ratio between the transitions is predicted to be 3.7. The comparison between the experimental results and the predictions of the calculations allows deducing that the accessible face (the most developed one of the crystal) is the *ac* face, which is shown in Figure 8 as taken from ref 14. Indeed, two different excitonic transitions are detected in the spectra taken at normal incidence, which are slightly shifted and orthogonally polarized. These bands are therefore attributed to the excitonic transitions (showing a vibronic progression) originating from the second

TABLE 1: Energies (E_m) and Oscillator Strength (f) of the Electronic Transitions Calculated by Osuna et al.[13] for the Single DBTDT Molecule and Energies and Components (in Debyes) along the Inertial Molecular Axes L, M, and N of the Electronic Transition Moments Calculated in This Work[a]

molecular electronic transitions						crystal excitonic transition		
E_m (eV)[13]	f[13]	E_m (eV)	L	M	N	b	a	c
3.77	0.69	3.86	6.72	0	0	13.44	0	0
3.89	0.07	3.95	0	2.10	0	0	1.93	0
						0	0	3.73
4.28	0.03	4.35	1.05	0	0	2.11	0	0
		4.69	0	1.12	0	0	1.04	0
						0	0	1.97
		4.84	2.25	0	0	4.51	0	0
		4.99	2.62	0	0	5.24	0	0

[a] For each molecular transition, the unit cell transition dipole moments (in Debyes) of the corresponding excitonic components at $k = 0$ (which are polarized along one of the unit cell axes) are also given.

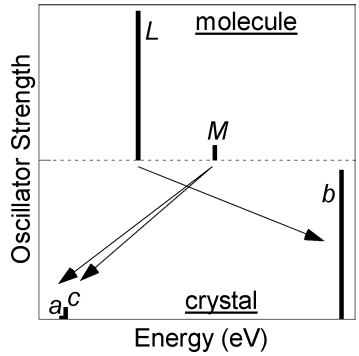

Figure 8. Schematic diagram showing the modifications from the single molecule to the crystal of the electronic transitions al lowest energy. The labels indicate the orientation of the corresponding transition moments with respect to the L, M, N molecular axes and with respect to the a, b, c crystal axes.

M-polarized molecular electronic transition (calculated at 3.95 eV in this work and at 3.89 by Osuna et al.).[13] The labels $E//c$ and $E//a$ in Figure 5 are derived from this attribution. The Davydov splitting between the corresponding replicas of the a and c progressions is found to be about 0.01 eV. Such a low value indicates that for this electronic transition the intermolecular interactions are relatively weak. At higher energy in Figure 5, broad and weaker bands are detected at about 4.21 and 5.07 eV and 4.21 and 5.08 eV for the two polarizations. These bands are attributed to other excitonic transitions in the ac plane of M molecular origin. For example, the bands at about 4.2 eV are attributed to the c and a excitonic transitions deriving from the molecular one calculated at 4.69 eV (the c-polarized band is more intense than the corresponding a-polarized band, as expected).

When varying the angle of incidence, the emerging band at 4.07 eV is attributed to the b polarized excitonic transition originating from the strongest transition of the single molecule at the lowest energy. This molecular transition has been calculated at 3.86 eV in this work and at 3.77 eV in ref 13 and has been observed at about 3.6 eV in the solution spectra.[13,14] The blue shift observed in the crystal spectra is explained by the arrangement of the corresponding L-molecular transition moments forming a pure H aggregate. We underline that polarized spectroscopy on monocrystals shows that there is no correspondence between the replicas observed at lowest energy in the solid state (originating from the second molecular transition) and the strong electronic transition at lowest energy of the single molecule. The diagram in Figure 8 schematically shows the modification of the first and second electronic states from the single molecule to the crystal.

To confirm the attribution of the transitions, we computed the relevant Davydov splittings using the Davydov theory of molecular excitons.[20] Excitonic bands at a given $\mathbf{k}$ can be found by diagonalizing the 4×4 resonance-interaction matrix defined as[20]

$$\tilde{J}_{\alpha\beta}(\mathbf{k}) = \sum_n{}' \exp(i\mathbf{k}n) J_{\alpha\beta}(\mathbf{n}) \quad (1)$$

where $J_{\alpha\beta}(\mathbf{n})$ is the interaction energy between a molecule of type α in cell $\mathbf{0} = (0, 0, 0)$ and a molecule of type β in cell $\mathbf{n}$. The primed summation indicates that self-interaction must be excluded, that is, if $\alpha = \beta$ then $\mathbf{n} \neq (0, 0, 0)$. Molecular interactions inside the crystal are often approximated to be interactions between point-dipoles located at the center of mass of each molecule. Such an approximation fails for molecules close to each other compared to their dimensions. To improve our estimate of such interactions, we used the transition charge distribution method, which consists in approximating the delocalized molecular dipole with a distribution of point charges located at atomic positions.[23,24] Such an approach gives a better accuracy for nearest neighbors interactions and, at the same time, allows the use of Ewald's method[20,25] to compute the sum in eq 1 for an infinite crystal, since for large $|\mathbf{n}|$ molecules are well described by point-dipoles. Transition charge distributions have been found as follows. From calculations based on time-dependent density-functional theory, we found that about 64% of the dipole moment of the first molecular transition comes from the HOMO/LUMO transition. So, we expressed the HOMO and LUMO wave functions as a sum of localized atomic orbitals and wrote the HOMO/LUMO transition dipole moment as the total dipole moment of a distribution of point-charges localized on atomic sites. To account for contributions from other orbitals, we finally normalized the dipole moment of the so obtained transition charge distribution to the computed transition dipole moment. The same procedure has been adopted for the second molecular transition, whose dipole moment is provided for more than 66% by the HOMO-1/LUMO transition. The transition charge distributions for the first two molecular transitions are reported in Figure 9.

We also included isotropic screening, so that the interaction energy between two molecules inside the crystal is finally given by[20]

$$J_{\alpha\beta}(\mathbf{n}) = \frac{1}{4\pi\varepsilon_0\varepsilon_s} \sum_{i,j} \frac{q_{i,\alpha} q_{j,\beta}}{\delta \mathbf{r}_{0i\alpha,\mathbf{n}j\beta}} \quad (2)$$

where ε_s is the static dielectric constant, chosen to be isotropic, $q_{i,\alpha}$ is the transition charge located on the ith atom of the αth

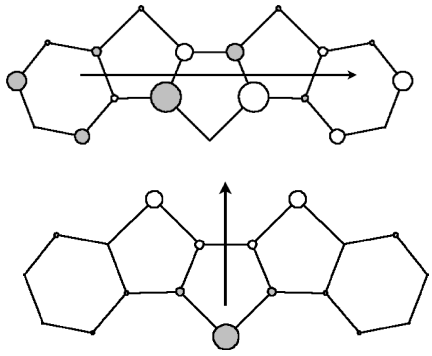

Figure 9. Transition charge distributions for the first two molecular transitions indicated by balls of increasing size. The arrows indicate the direction of the resulting transition dipole moment.

molecule, and $\delta\mathbf{r}_{0i\alpha,\mathbf{n}j\beta}$ is the distance between the ith atom of the αth molecule in cell **0** and the jth atom of the βth molecule in cell **n**. In the present work, we used a screening dielectric constant $\varepsilon_s = 3$, which is in agreement with the values commonly adopted for similar molecules such as pentacene.[22,26,27] The sum in eq 1 was computed for an infinite three-dimensional crystal in two steps: first we used the point dipole-point dipole approximation and made use of the Ewald's procedure to obtain convergence of the sum and then we replaced point dipole-point dipole interactions with the more accurate expression of eq 2 whenever the distance between the centers of mass of two molecules was less than a cutoff distance r_{max}. In our calculations we used $r_{max} = 100$ Å, which was enough to achieve convergence of the energy bands.

It is well-known that in three-dimensional crystals the energies of the excitonic bands are nonanalytic functions of $\mathbf{k}$ as $\mathbf{k}\rightarrow 0$.[20] For this reason, to compare our predictions with the experimental results, we computed $\tilde{J}^{DS}_{\alpha\beta} = \lim_{k\rightarrow 0} \tilde{J}_{\alpha\beta}(\mathbf{k}_{//b})$, that is, we considered incident light coming along a direction perpendicular to the crystal exposed face. By diagonalizing $\tilde{J}^{DS}_{\alpha\beta}$ we could finally find the purely excitonic energies as probed by absorption at normal incidence. Numerical calculations based on the method described above predicted in the case of the first molecular transition was found to be a Davydov splitting of 0.44 eV between the dark exciton at lowest energy and the allowed *b*-polarized upper exciton, while for the second molecular transition the Davydov splitting between the two allowed excitons was found to be 0.002 eV, thus confirming the weak intermolecular interaction of the second *M*-polarized molecular electronic transition. This suggests that the lowest excitonic transition (dark) coming from the first molecular transition is expected to be about at the same energy as the excitonic transitions detected in the normal-incidence spectra, which comes from the second molecular *M* transition.

We stress that the theoretical approach that we adopted takes full account of all the crystal symmetries, including of course the translational symmetry, from which all the qualitative features of the excitonic absorption spectra arise. In addition, the numerical calculations described above provide a fairly accurate description of the dispersion of the purely excitonic bands and allow a quantitative comparison with experiments.[20−24,27] We are aware that a more accurate estimate of the molecular interactions can be obtained by quantum mechanical calculations involving several molecules. Nevertheless such a refinement would be relevant only for nearest-neighbor or next-nearest-neighbor molecules and would only slightly correct the Davydov splitting values without affecting the main conclusions of the present work.

The experimental results and the interpretation based on theoretical considerations suggest a simple method to deduce information about the structural/morphological properties of different types of DBTDT samples, such as polycrystalline thin films. For example, Gao et al.[7] report the absorption spectrum of a thin film. The observed progression at lowest energy is clearly observed, while no experimental evidence is found of the excitonic transition at about 4.07 eV. Since the measurements were performed at normal incidence on the film, this clearly indicates that the plane of the films deposited on quartz is the *ac* plane. This information was obtained by the authors[7] by means of X-ray diffraction measurements on the films deposited on octadecyl-trichlorosilane-treated SiO_2/Si substrates. Our analysis of the optical properties of the monocrystals provides a simple method to deduce information on the crystallinity and, in particular, on the orientation of the molecules and of the unit cell axes with respect to the substrate. For applications in thin-film transistors, this is fundamental: the orientation must be favorable for achieving high mobility because the stacking direction is consistent with the direction of current flow. A similar approach was used also in the case of oligothiophenes films.[21] Optical absorption technique at oblique incidence has been used to experimentally recognize the macroscopic order and structural features of samples of quaterthiophene from single crystals to polycrystalline or twinned samples.

Conclusions

In this work, we have performed the organic synthesis and the growth of DBTDT single crystals. From the UV−visible polarized absorption analysis at normal and oblique incidence it was possible to definitely attribute the observed bands and their polarizations, on the basis of the molecular and crystal geometry. We underline that, in the crystal, the molecular arrangement gives rise to either a pure H aggregate or a herringbone aggregate, for the electronic molecular transition at lower energy or the following one, respectively. The different arrangement and the different strength of the intermolecular interactions cause different Davydov splitting. In particular, the excitonic transitions at lowest energy in the crystal originate from the second electronic transition of the molecule (arranged in a herringbone configuration), while the one at lowest energy of the single molecule gives rise to a blue shifted and relatively strong excitonic state of pure H-type at higher energy. The largest crystal face was attributed on the basis of the spectroscopic results. Taking into consideration the origin of the different optical bands, which is provided here, the same simple approach is proposed to determine the exposed face and the structural/morphological properties of different types of DBTDT samples, such as polycrystalline thin films, important for device applications.

Acknowledgment. We are pleased to thank Marcello Campione for assistance in the crystal growth, Silvia Trabattoni for assistance in atomic force microscopy, and *Fondazione Cariplo* for financial support.

Supporting Information Available: Description of the organic synthesis and characterization. This material is available free of charge via the Internet at http://pubs.acs.org.

References and Notes

(1) Anthony, J. E. *Chem. Rev.* **2006**, *106*, 5028–5048.
(2) Anthony, J. E. *Angew. Chem. Int. Ed.* **2008**, *47*, 452–483.
(3) Bendikov, M.; Wudl Perepichka, D. F. *Chem. Rev.* **2004**, *104*, 4891–4945.

(4) Jurchescu, O. D.; Baas, J. M.; Palstra, T. T. *Appl. Phys. Lett.* **2004**, *84*, 3061–3063.

(5) Maliakal, A.; Raghavachari, K.; Katz, H.; Chandross, E.; Siegrist, T. *Chem. Mater.* **2004**, *16*, 4980–4986.

(6) Li, X.-C.; Sirringhaus, H.; Garnier, F.; Holmes, A. B.; Moratti, S. C.; Feeder, N.; Clegg, W.; Teat, S.; Friend, R. H. *J. Am. Chem. Soc.* **1998**, *120*, 2206–2207.

(7) Gao, J.; Li, R.; Li, L.; Meng, Q.; Jiang, H.; Li, H.; Hu, W. *Adv. Mater.* **2007**, *19*, 3008–3011.

(8) Szperl, L. *Rocz. Chem.* **1938**, *18*, 804–811.

(9) (a) Klauk, H.; Halik, M.; Zschieschang, U.; Schmid, G.; Radlik, W.; Weber, W. *J. Appl. Phys.* **2002**, *92*, 5259–5263. (b) Sheraw, C. D.; Zhou, L.; Huang, J. R.; Gundlach, D. J.; Jackson, T. N.; Kane, M. G.; Hill, I. G.; Hammond, M. S.; Campi, J.; Greening, B. K.; Francl, J.; West, J. *Appl. Phys. Lett.* **2002**, *80*, 1088–1090. (c) Gundlach, M. S.; Lin, Y. Y.; Jackson, T. N.; Nelson, S. F.; Schlom, D. G. *IEEE Electron Device Lett.* **1997**, *18*, 87–89.

(10) (a) Yamada, M.; Ikemoto, I.; Kuroda, H. *Bull. Chem. Soc. Jpn.* **1988**, *61*, 1057–1062. (b) Coppo, P.; Yeates, S. G. *Adv. Mater.* **2005**, *17*, 3001–3005. (c) Meng, H.; Bendikov, M.; Mitchell, G.; Helgeson, R.; Wuld, F.; Bao, Z.; Siegrist, T.; Kloc, C.; Chen, C. H. *Adv. Mater.* **2003**, *15*, 1090–1093.

(11) Wex, B.; Kaafarani, B. R.; Kirschbaum, K.; Neckers, D. C. *J. Org. Chem.* **2005**, *70*, 4502–4505.

(12) Xiao, K.; Liu, Y.; Qi, T.; Zhang, W.; Wang, F.; Gao, J.; Qiu, W.; Ma, Y.; Cui, G.; Chen, S.; Zhan, X.; Yu, G.; Qin, J.; Hu, W.; Zhu, D. *J. Am. Chem. Soc.* **2005**, *127*, 13281–13286.

(13) Osuna, R. M.; Ortiz, R. P.; Okamoto, T.; Suzuki, Y.; Yamaguchi, S.; Hernandez, V.; Navarrete, J. T. L. *J. Phys. Chem. B* **2007**, *111*, 7488–7496.

(14) Okamoto, T.; Kudoh, K.; Wakamiya, A.; Yamaguchi, S. *Org. Lett.* **2005**, *7*, 5301–5304.

(15) Szperl, L. *Rocz. Chem.* **1938**, *18*, 804.

(16) Schroth, W.; Hintzsche, E.; Jordan, H.; Jende, T.; Spitzner, R.; Thondorf, I. *Tetrahedron* **1997**, *53*, 7509.

(17) Campione, M.; Ruggerone, R.; Tavazzi, S.; Moret, M. *J. Mater. Chem.* **2005**, *15*, 2437–2443.

(18) Frisch, M. J.; Trucks, G. W.; Schlegel, H. B.; Scuseria, G. E.; Robb, M. A.; Cheeseman, J. R.; Montgomery, J. A.; Vreven, T.; Kudin, K. N.; Burant, J. C.; Millam, J. M.; Iyengar, S. S.; Tomasi, J.; Barone, V.; Mennucci, B.; Cossi, M.; Scalmani, G.; Rega, N.; Petersson, G. A.; Nakatsuji, H.; Hada, M.; Ehara, M.; Toyota, K.; Fukuda, R.; Hasegawa, J.; Ishida, M.; Nakajima, T.; Honda, Y.; Kitao, O.; Nakai, H.; Klene, M.; Li, X.; Knox, J. E.; Hratchian, H. P.; Cross, J. B.; Bakken, V.; Adamo, C.; Jaramillo, J.; Gomperts, R.; Stratmann, R. E.; Yazyev, O.; Austin, A. J.; Cammi, R.; Pomelli, C.; Ochterski, J. W.; Ayala, P. Y.; Morokuma, K.; Voth, G. A.; Salvador, P.; Dannenberg, J. J.; Zakrzewski, V. G.; Dapprich, S.; Daniels, A. D.; Strain, M. C. Farkas, O.; Malick, D. K.; D. Rabuck, A.; Raghavachari, K.; Foresman, J. B.; Ortiz, J. V.; Cui, Q.; Baboul, A. G.; Clifford, S.; Cioslowski, J.; Stefanov, B. B.; Liu, G.; Liashenko, A.; Piskorz, P.; Komaromi, I.; Martin, V. D.; Fox, J.; Keith, T.; Al-Laham, M. A.; Peng, C. Y.; Nanayakkara, A.; Challacombe, M.; Gill, P. M. W.; Johnson, B.; Chen, W.; Wong, M. W.; Gonzalez,; Pople, J. A. *Gaussian 03*, Revision D.02; Gaussian, Inc.: Wallingford, CT, 2004.

(19) Born, M. Wolf, E. *Principle of Optics*; Cambridge University Press: New York, 1999.

(20) Davydov, A. S. *Theory of Molecular Excitons*; Plenum: New York, 1971.

(21) (a) Spearman, P.; Borghesi, A.; Campione, M.; Laicini, M.; Moret, M.; Tavazzi, S. *J. Chem. Phys.* **2005**, *122*, 014706. (b) Raimondo, L.; Campione, M.; Laicini, M.; Moret, M.; Sassella, A.; Spearman, P.; Tavazzi, S. *Appl. Surf. Sci.* **2006**, *253*, 271–274. (c) Tavazzi, S.; Laicini, M.; Raimondo, L.; Spearman, P.; Borghesi, A.; Papagni, A.; Trabattoni, S. *Appl. Surf, Sci.* **2006**, *253*, 296–299. (d) Tavazzi, S.; Campione, M.; Laicini, M.; Raimondo, L.; Borghesi, A.; Spearman, P. *J. Chem. Phys.* **2006**, *124*, 194710.

(22) Silvestri, L.; Tavazzi, S.; Spearman, P.; Raimondo, L.; Spano, F. C. *J. Chem. Phys.* **2009**, *130*, 234701.

(23) Scholz, R.; Kobitski, A.; Kampen, T.; Schreiber, M.; Zahn, D.; Jungnickel, G.; Elstner, M.; Sternberg, M.; Frauenheim, T. *Phys. Rev. B* **2000**, *61*, 13659.

(24) Vragovic, I.; Scholz, R. *Phys. Rev. B* **2003**, *68*, 155202.

(25) Philpott, M. R.; Lee, J. W. *J. Chem. Phys.* **1973**, *58*, 595.

(26) Kang, H. S.; Lee, J. W.; Kim, M. K.; Joo, J.; Ko, J. M.; Lee, J. Y. *J. Appl. Phys.* **2006**, *100*, 064508.

(27) Garnier, F.; Yassar, A.; Hajlaoui, R.; Horowitz, G.; Deloffre, F.; Servet, B.; Ries, S.; Alnot, P. *J. Am. Chem. Soc.* **1993**, *115*, 8716–8721.

JP1052826